Journal of Magnetic Resonance 349 (2023) 107405

Contents lists available at ScienceDirect

Journal of Magnetic Resonance

journal homepage: www.elsevier.com/locate/jmr

Operando NMR metabolomics of a microfluidic cell culture

Genevieve Rogers [a], Sylwia Barker [b], Manvendra Sharma [b], Salim Khakoo [a], Marcel Utz [b,*]

[a] School of Medicine, University of Southampton, Tremona Road, Southampton, SO17 1BJ Hampshire, UK
[b] School of Chemistry, University of Southampton, Highfield Campus, Southampton, SO17 1BJ Hampshire, UK

ARTICLE INFO

Article history:
Received 19 December 2022
Revised 9 February 2023
Accepted 12 February 2023
Available online 21 February 2023

Keywords:
Microfluidic NMR
Cell culture
Hepatocellular carcinoma (HCC)
Lab-on-a-chip
Metabolomics

ABSTRACT

In this work we demonstrate the use of microfluidic NMR for *in situ* culture and quantitative analysis of metabolism in hepatocellular carcinoma (HCC) cell lines. A hydrothermal heating system is used to enable continuous *in situ* NMR observation of HCC cell culture over a 24 h incubation period. This technique is nondestructive, non-invasive and can measure millimolar concentrations at microlitre volumes, within a few minutes and in precisely controlled culture conditions. This is sufficient to observe changes in primary energy metabolism, using around 500–3500 cells per device, and with a time resolution of 17 min. The ability to observe intracellular responses in a time-resolved manner provides a more detailed view of a biological system and how it reacts to stimuli. This capability will allow detailed metabolomic studies of cell-culture based cancer models, enabling quantification of metabolic reprogramming, the metabolic tumor microenvironment, and the metabolic interplay between cancer- and immune cells.

© 2023 The Author(s). Published by Elsevier Inc. This is an open access article under the CC BY license (http://creativecommons.org/licenses/by/4.0/).

1. Introduction

Cancer cell metabolism is widely known to be reprogrammed following tumourigenesis. Despite early observations by Warburg [1] and his peers, the significance and potential for exploitation of these alterations were not fully appreciated until more recently. Tumour cell metabolism is now recognised as a potential molecular target for anti-cancer therapies [2,3]. ^{1}H nuclear magnetic resonance (NMR) spectroscopy is a powerful tool for the quantification of the metabolism of living systems. Its biocompatibility is exploited by *in vivo* studies in the context of magnetic resonance imaging [4–6]. In-vivo high-resolution NMR spectroscopy, where either cells or entire organisms are present in the NMR sample, has made it possible to study biomolecules in their native environment [7] and is widely used in the context of drug discovery [8] as well as for environmental studies; Lane et al. [9,10] have observed the response of the metabolism of Daphnia magna to environmental pollutants in this way. In-vivo NMR has also been widely used to observe metabolism in cell cultures [11–14]. Microfluidic lab-on-a-chip (LoC) devices [15] are increasingly finding applications in life science research [16], for example in the form of organoid [17] or organ-on-a-chip systems [18]. They allow working with minimal sample volumes, can integrate complex experimental protocols on a single, expendable platform, and, crucially, allow for detailed control over environmental conditions in cultures of cells, cell aggregates, and tissue samples. Several techniques exist to monitor metabolism in culture systems, including liquid-chromatography/mass spectrometry (LC-MS) [19], Extracellular Flux (XF) analysis (Seahorse Bioscience) [20,21] for measurement of extracellular acidification rate (ECAR) and oxygen consumption rate (OCR) of intact cells, as well as NMR spectroscopy [22,23,11]. While MS-based techniques are usually destructive due to the need to ionize the sample, extracellular flux analysis is highly specific, focusing on only a very small number of parameters such as pH and oxygen consumption. Due to its ability to broadly quantify metabolites in living systems with minimal interference, NMR spectroscopy is in principle an ideal tool to follow metabolism in LoC cultures. However, this has so far only rarely been demonstrated due to a number of challenges: LoC systems work with sample volumes on the order of pL to several μL, while conventional liquid-state NMR systems use samples ranging from 50 μL to 600 μL. The planar shape factor of microfluidic devices is at odds with the cylindrical detection volume of standard NMR probes. Finally, differences in magnetic susceptibility between microfluidic chip materials and the fluid to be detected can lead to inhomogeneous line broadening and a loss of resolution.

Many of these issues have recently been addressed by the development of planar microfluidic NMR detectors based on strip lines [24], transmission lines [25] and micro-fabricated Helmholtz coil pairs [26]. These systems benefit from favourable scaling of mass sensitivity of NMR detectors with decreasing detection volume, which is a consequence of more intimate coupling between

* Corresponding author.
E-mail address: marcel.utz@gmx.net (M. Utz).

https://doi.org/10.1016/j.jmr.2023.107405
1090-7807/© 2023 The Author(s). Published by Elsevier Inc.
This is an open access article under the CC BY license (http://creativecommons.org/licenses/by/4.0/).

the precessing nuclear spin magnetization and the detection structure [27]. Microfluidic cell cultures have been observed in such systems before. Kalfe et al. [28] have used a stripline detector to quantify the metabolic turnover of a cell spheroid. This work used a glass microfluidic device with an oxygen supply and heating system to obtain metabolic data from a single spheroid of approximately 9000 cells over a 24 h period. Recently, Patra et al. have compared the metabolism of MCF-7 cells in microfluidic adherent and spheroid culture [29]. In this work, between 1200 and 2000 cells were cultured on a microfluidic chip and the concentrations of 12 different metabolites were determined at intervals of 4 h or 8 h. In between these measurements, the chips with the cells were kept in an incubator, from which they were periodically removed and manually inserted into the NMR spectrometer equipped with a modular transmission line probe designed to accommodate the LoC devices [25].

Liver cancer is one of the most common cancers worldwide and is the third most common cause of cancer death [30]. Hepatocellular carcinoma (HCC) is the most common type of primary liver cancer, accounting for 75–85% of cases. Furthermore, liver cancer prevalence is a growing problem: over the last ten years incidence rates have increased by 52% and are predicted to rise by a further 43% for males and 21% for females in the UK between 2014 and 2035 [31]. This disease has a diverse range of causes, but commonly occurs in the context of liver fibrosis due to chronic liver disease such as non-alcoholic fatty liver disease (NAFLD), alcohol liver disease or chronic viral hepatitis [30]. Only 13% of people diagnosed with liver cancer in England survive past five years after diagnosis [31]. HCC is often diagnosed only in the advanced stages of disease, ruling out surgery as an option and contributing to the low survival rate [32]. Additionally, in these later stages, the ability to metabolise chemotherapeutic agents is reduced, leading to poor tolerance of chemotherapy. Immunotherapy has therefore become a promising potential treatment for HCC. However, there is evidence to suggest that the metabolic microenvironment of the tumour leads to suppression of cytotoxic immune cell activity and prevents killing of cancer [33–35]. Quantification of metabolic activity is therefore of great importance for microfluidic studies of the interaction between HCC cell lines and immune cells.

In the present contribution, we enable continuous NMR monitoring of microfluidic cell cultures. This requires additional hardware provisions for the microfluidic probe in order to ensure isothermal conditions for the culture. As will be discussed in the following, it was technically challenging to ensure stable operation of the probe and culture system over periods of up to 24 h to allow quantitatively consistent metabolite concentration readouts. The required provisions in terms of internal standards, water suppression, and operation of the microfluidic system will be discussed in detail.

Our ultimate objective was to quantify the remodelling of cellular metabolism in hepatocellular carcinoma cell lines to determine if there are differences correlating to cell line, the level of malignancy, or the stage of disease advancement.

2. Microfluidic NMR system

In this work we demonstrate a microfluidic platform for *in situ operando* metabolic NMR analysis of live cells. The entire setup, shown in Fig. 1, consists of a home-built transmission-line NMR probe [36], a microfluidic chip fabricated from PMMA sheets by laser cutting and thermal bonding and a pair of fluidic holders that clamp the chip and provide threaded connections for 1/16" capillaries. Microfluidic devices contain a 2.5μL sample chamber that is aligned with the NMR detector structure. Channels of 100μm depth connect the sample chamber to inlets/outlets at the top of the device (Fig. 1D). A pair of heating sleeves was used to control temperature at the sample chamber. As shown in Fig. 1B, the sleeves are arranged symmetrically around the conductor planes of the probe and are perfused with warm water using an external thermostat system. The accuracy of this system was verified using the chemical shift difference between water and DSS as an NMR thermometer. Fig. 1E shows the correlation between the measured sample temperature and the heater setpoint. The sample chamber temperature follows the set temperature with better than 1°C accuracy. Fig. 1F shows the thermal stability of the system; fluctuations are less than 0.1°C.

3. Materials and methods

Chip, fluidic holders, heating sleeve design and fabrication. Microfluidic LoC devices were fabricated from three layers of polymethyl methacrylate (PMMA) (Weatherall Equipment, Wendover, UK), the middle layer is 500μm thick while the top and bottom layers are each 200μm thick. A laser engraving system (HPC Laser LTD, Elland, UK) was used to score the required microfluidic design into PMMA, creating 150μm depth and width microfluidic channels. Devices were bonded together using a combination of 5% v/v dibutyl phthalate (DBP) plasticiser in isopropanol and thermal bonding, as described previously [37]. To pressurise the microfluidic system, devices are overlaid with laser cut polydimetylsiloxane (PDMS) (Shielding Solutions, UK) gaskets and held together with a pair of fluidic holders using four brass M3 screws. The holders and sleeves were custom-designed using SolidWorks, and fabricated by 3D printing (Protolabs Ltd, UK). Nanoport connectors (IDEX Ltd., UK) are used to connect 0.8 mm/1/16" ID/OD Polytetrafluoroethylene (PTFE/Teflon) tubing (Sigma Aldrich, US) to the fluidic holders and to the heating sleeves.

Thermal control. The heating system is external to the probe and contains a peristaltic pump, resistive heater with a maximum power rating of 50 W, and an arduino Mega 2560 microcontroller. The heating sleeves have an internal volume of 20 ml each. During experiments, a flow rate of approximately 20 ml/min was maintained continuously, leading to a residence time of about 2 min. A proportional-integral–differential control loop is implemented using the arduino software, making use of the readout of the PT 1000 thermal sensor located in one of the heating sleeves, as discussed above. Safety precautions were programmed into the heater including a smoke detector and measures to shut off the power if smoke is detected or if the power is running at 100% for a sustained period of time.

NMR Measurements. A Bruker 11.7T NMR spectrometer, corresponding to a proton resonance frequency of 500 MHz, with an Avance III console was used to obtain ^{1}H spectra. A home-built transmission line NMR probe was used, specifically designed to accommodate the microfluidic device shape [36]. The same probe had already been used to observe the metabolism in microfluidic cultures of MCF-7 cells [11]. Detailed CAD drawings for the mechanical and electronic design of this probe are freely available in a public repository at https://github.com/marcel-utz/modular-microfluidic-probe. Spectra were acquired using the PROJECT sequence [38] using 64 echoes with a total echo delay of 128 ms. Water signals were suppressed using CW presaturation. The 90° pulse was calibrated to 3.5μs at 50 W power, corresponding to a nutation frequency of 71 kHz. CW water presaturation was applied throughout the recycle delay time of 3s at 5×10^{-5} W power. 16 k data points were acquired over a spectral width of 20 ppm. For each spectrum, 256 scans were averaged over a period of 17.5 min; this led to 82 spectra for an approximately 24 h culture experiment.

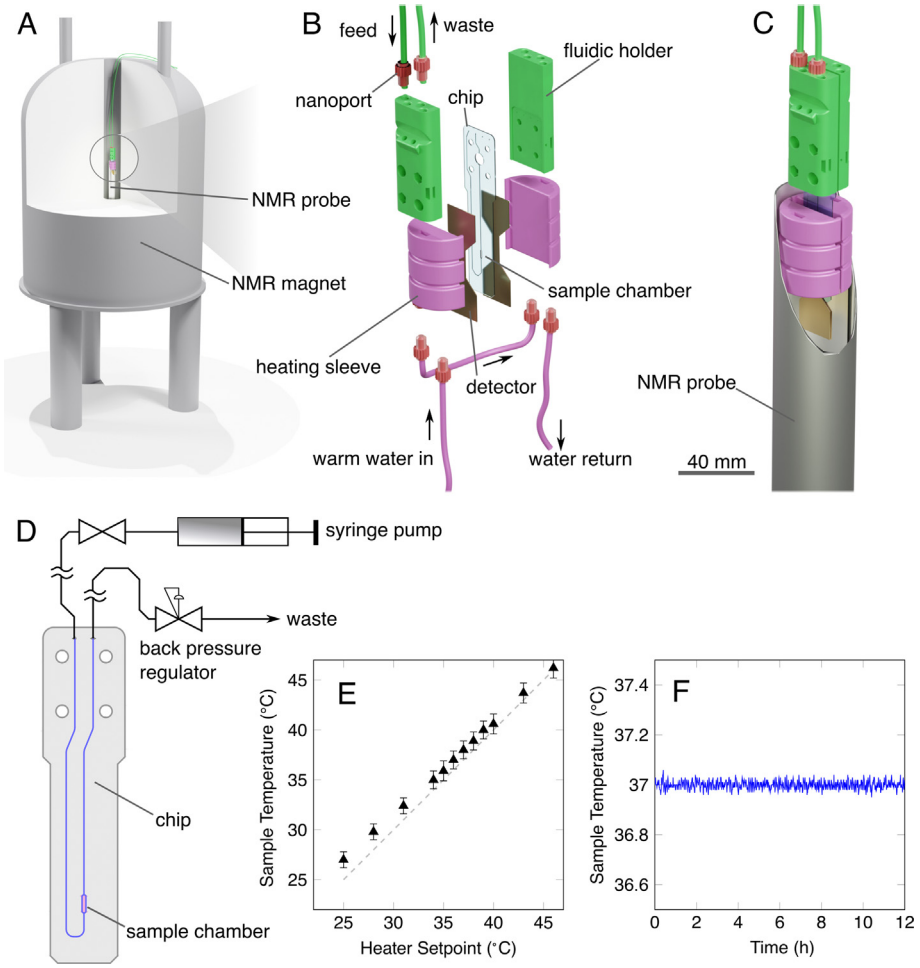

Fig. 1. A) Schematic rendering of the TLP probe inside the NMR magnet (left). B) The microfluidic chip is positioned between the detector planes of the TLP probe (centre), which in turn are surrounded by two heating sleeves. C) The chip is clamped between two fluidic holders, which provide threaded connections for standard 1/16" fluidic capillaries, D) used to fill the device by syringe pump and to apply back-pressure. E) Temperature calibrations and F) temperature stability.

NMR data were processed using home-built routines written in Julia [39]. Free induction decays were zero-filled to 32 k points, and apodized with 1 Hz of Lorentzian line broadening.

Magnetic Resonance Imaging. MRI gradient echo images of the microfluidic device sample chamber were obtained at 11.7T using a Bruker micro-imaging gradient system. ParaVision software was used with the fast low-angle shot (FLASH) pulse program, a repetition time of 800 ms and average of 4 scans. Two images were taken, with echo times of 4 ms and 20 ms, and the local field was determined from the difference in the signal phase at each pixel across the sample chamber.

Cell culture. Two HCC cell lines were used; PLC and HepG2 (ATCC, UK), cultured in DMEM (Thermo Fisher Scientific, UK) with 10% FBS (Sigma Aldrich, US) and 5% penicillin/streptomycin (Life Technologies, US). To avoid complications due to the decomposition of GlutaMAX into alanine and glutamine, which may falsely indicate production of these amino acids, media without GlutaMAX but with L-Glutamine was used.

For culture in LoC devices, sample chambers were washed with PBS (Thermo Fisher Scientific, UK), coated with 10μL of 1 mg/ml bovine plasma fibronectin (Thermo Fisher Scientific, UK) overnight and UV sterilised for 30 min in a biosafety cabinet. HCC cells were seeded at 750 cells/μL with 25 mM deuterated HEPES (Cambridge Isotope Laboratories, UK) and either 3 mM DSS or later 2 mM DMSO (Sigma Aldrich, US) as an internal reference compound. Devices were filled using a syringe pump at 30μL/min (Fig. 1D). Once filled, the gate valve between device and syringe is closed and back pressure is applied at 1.2 bar throughout the experiment (1D). Microfluidic devices were then incubated inside the NMR probe at 37°C for one hour to allow cell adhesion before ^{1}H NMR spectroscopy for 24 h.

Images of the cells at the sample chamber were taken using an inverted microscope with a 10X objective, equipped with a RaspberryPi camera before and after culture. Three images were taken to span the entire length of the sample chamber, and cell numbers were counted and recorded to be later used to determine per cell metabolic rates.

Cell viability was verified using a fluorescent LIVE/DEAD^{TM} viability stain (Invitrogen, US) and fluorescence microscopy (data not shown). NMR experiments were run in triplicate, with new devices for each experiment. Media controls were carried out using 3 mM DSS (Sigma Aldrich, US) as an internal reference compound, later changed to 2 mM DMSO to lessen cellular toxicity.

4. Results and discussion

Fig. 2A illustrates a typical NMR spectrum obtained from this microfluidic *in operando* culture system. As all spectra reported here, it was recorded in 256 scans over a period of 17.5 min. The spectral resolution, measured by the line width of the DMSO signal, is 6 Hz. The signal-to-noise ratio (SNR) of the DMSO peak is 95.9, from which the number limit of detection was determined [40]

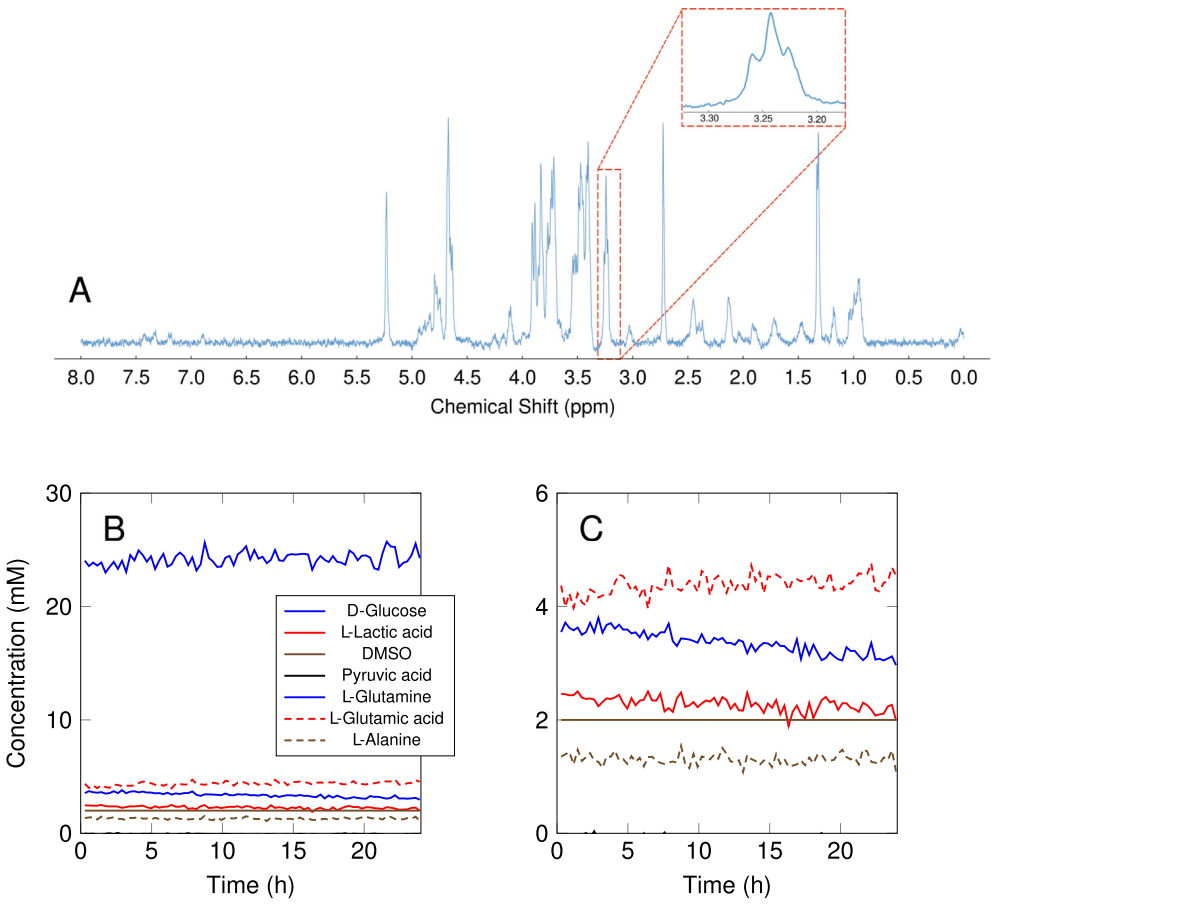

Fig. 2. Data quality: A) A typical spectrum acquired from culture media, with an inset showing a glucose triplet at higher magnification. B) Concentration of six metabolites in control experiments, without cells, for 24 h. C) same as B), vertical scale expanded.

as nLOD = 1.01 nmol$\sqrt{s}$ and the concentration limit of detection of cLOD = 4.06mM$\sqrt{s}$; Sharma and Utz had characterized the performance of this probe at 600 MHz and with a different reference compound (Acetate), and reported nLOD = 1.4 nmol$\sqrt{s}$. The slight improvement observed in the present work may be due to somewhat better efficiency of the tuning and matching network at 500 MHz. The spectrum shows signals from a wide variety of metabolites, mainly in the region between 0.5 ppm and 5.5 ppm. Weak signals stemming from aromatic amino acids are also visible between 6.5 ppm and 7.5 ppm. The anomeric signals of α- and β-glucose, at 5.5 ppm and 4.6 ppm, respectively, are also clearly visible. The broad feature between 4.5 and 5.0 ppm corresponds to imperfect water suppression, which is notoriously difficult in these microfluidic systems due to distant water in channels other than the sample chamber itself.

Fig. 2B describes a control experiment in which the sample chamber was filled with culture media but without cells. This plot shows the concentrations of 6 metabolites, plus DMSO as an internal standard, over the course of a 24 h control experiment. All metabolite concentrations fluctuate about a constant mean value, with the exception of L-Glutamine, which decays by about 30% over the course of 24 h, reflecting its well-known decomposition into ammonia and pyrrolidone-carboxylic acid at this temperature and pH [41]. Quantitative stability of the spectra and the resulting metabolite concentrations is a technical requirement for metabolic monitoring of cell cultures. Stable results like the ones shown in Fig. 2B were initially difficult to achieve. Fig. 3A shows the DSS

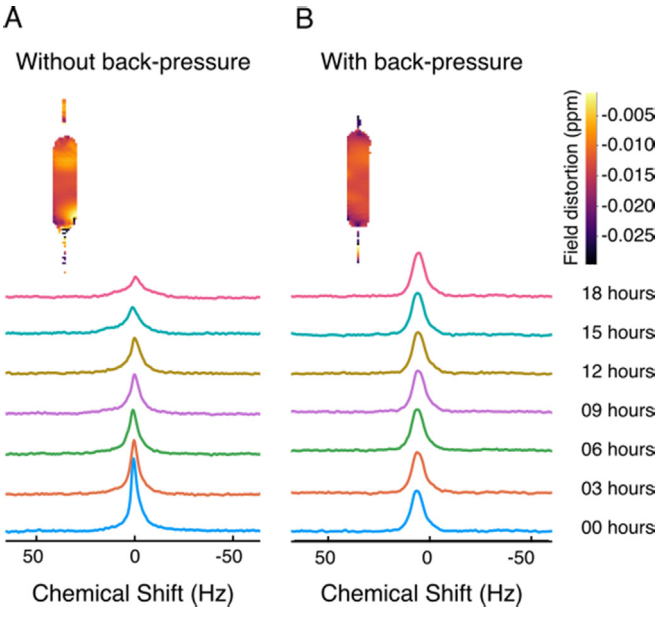

Fig. 3. Signal instability caused by bubble formation was improved by pressurisation. A) without pressurisation of the microfluidic system, local magnetic field distortion caused peak broadening and signal loss. B) with back pressure application this issue was avoided. Inset images show a field map of the sample chamber both with and without back pressure application.

signal as a function of time in an early experiment. As the figure shows, the signal gradually broadens with time, and some of its intensity starts to be lost in the noise. This behaviour, which affected all spectral lines, caused spurious drifts in the metabolite concentrations. Gradual formation of gas bubbles in the sample chamber, causing magnetic field distortions (see field map in the inset of Fig. 3A), were eventually identified as the source of this behaviour. While degassing prior to the experiments alleviated this problem in the case of the controls, this was not sufficient in the case of cell cultures, most likely due to formation of CO_2 gas as a result of metabolic activity of the cells. Ultimately, the problem was resolved by applying 1.2 bar of back pressure on the waste channel of the chip. In this way, the liquid was kept under at least 1 bar above atmospheric pressure, and bubble formation remained suppressed. This is illustrated in the field map and the stability of the DMSO peak shown in Fig. 3B.

Metabolite concentrations were obtained from the spectra by linear decomposition using reference peak positions and intensities from the Human Metabolome Database (HMDB) [42]. The process has been described in detail elsewhere [29]. The decomposition is illustrated in Fig. 4A. Briefly, elementary spectra for each metabolite of interest were computed from the HMDB data using the same digital resolution and approximate line width as the experimental spectra. The concentrations were then obtained by finding an optimal representation of the experimental spectrum. The resulting fit is shown along with the experimental spectrum at the top of Fig. 4A. It represents the experimental spectrum very well, in the sense that almost all visible signals in the experimental spectrum are also present in the fit. Notable exceptions are the signal at 1.2 ppm, which is due to traces of isopropanol left over from chip fabrication, and a small signal at 3.1 ppm, which we suspect is due to exchanged protons in the deuterated HEPES buffer. Absolute concentrations were obtained by calibration against the known concentration of DMSO in each spectrum. This was repeated for each of 82 spectra in a 24 h data set, yielding concentrations as a function of time with a resolution of 17 min. The control data shown in Fig. 2 have also been obtained in this way. The signal from the anomeric proton of β-D-Glucose, a doublet that appears

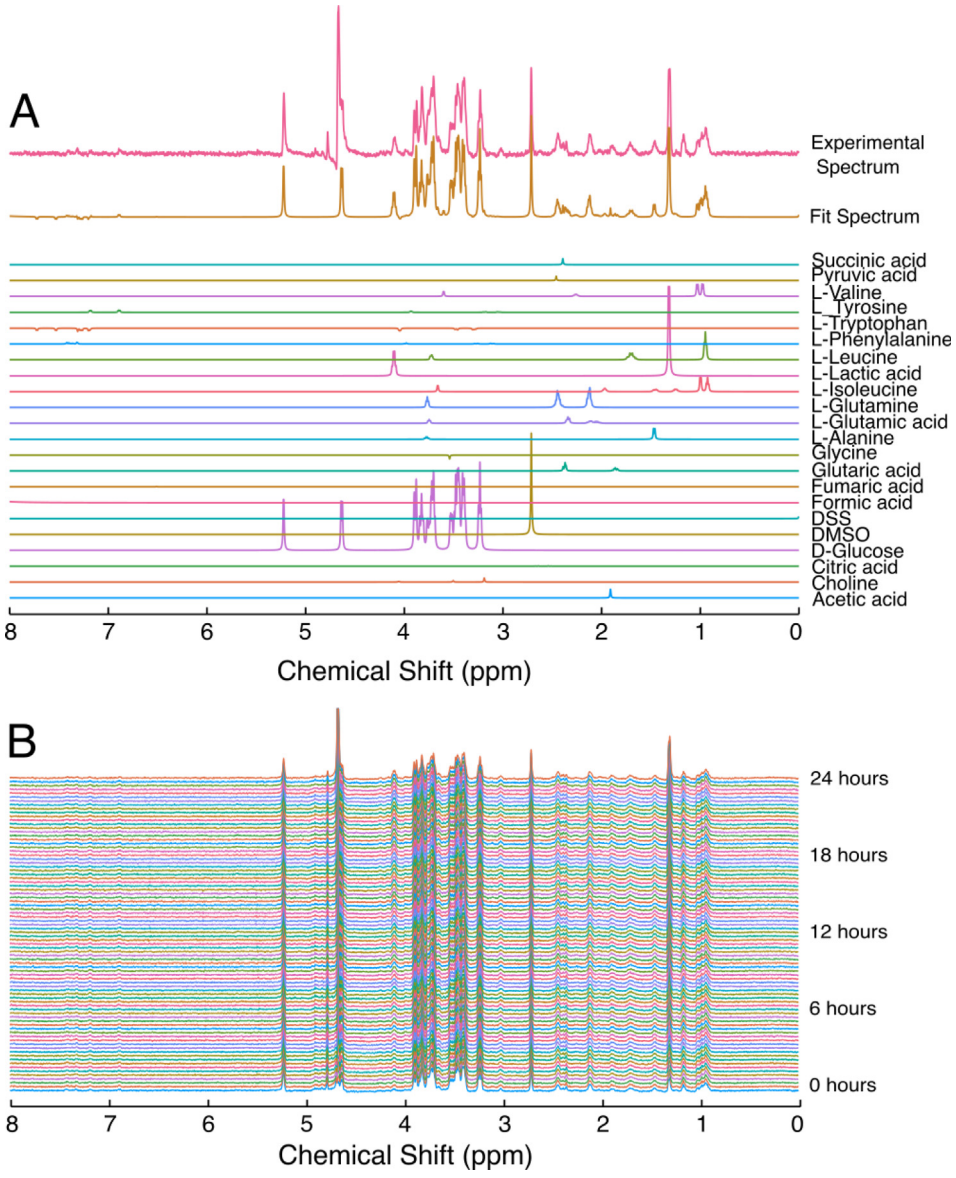

Fig. 4. Decomposition of a proton NMR spectrum; A) individual metabolite spectra are quantitative reference spectra (QRS), normalised to the same concentration. The weighted sum of the QRS builds the fit spectrum, which can be used as a comparison of the experimental spectrum. B) 82 spectra, recorded over 24 h. Spectral decomposition is applied to each to determine changes in metabolite signals.

at 4.6 ppm, overlaps with the imperfectly suppressed water signal. To avoid distortion of the reported Glucose concentration, the doublet at 4.6 ppm was therefore omitted from the reference spectrum used for the calculation of the concentrations.

Images of the sample chamber were taken at 0hrs and at the end of the 24 h experiment. Three overlapping images were taken, spanning the entire area of the sample chamber, a subset of which are shown in Fig. 5.

HCC cells were cultured within the pressurised microfluidic NMR system and observed *in situ* for 24 h. Phase contrast micrographs of the cultures of PLC and HepG2 cells are shown in Fig. 5. The cells attach and spread out on the chip surface and proliferate somewhat over 24 h. Coverage is less than a monolayer in both cases. 82 spectra were generated over 24 h, and integration of metabolite peaks reveals changes in concentration. The grey solid lines in Fig. 6 A and B represent the resulting time-concentration profiles for each metabolite; the smoothed profiles shown in color in Fig. 6 have been obtained by Tikhonov regularization as explained below.

The greatest changes in extracellular concentration from PLC cell culture are seen in glucose and lactic acid, in line with the highly glycolytic nature of these cells. Over the 24 h period, the cells consumed 7 mM of D-Glucose and produced 14 mM of L-Lactic acid. Glucose is taken up by cells via glucose transporters, GLUT1 and Glut2, both of which are upregulated in HCC [43]. Glucose is then converted via a 10-step process of glycolysis to cytosolic pyruvate. One molecule of glucose creates 2 molecules of pyruvate. In healthy cells in abundant oxygen, the majority of pyruvate moves into the mitochondria and into the TCA cycle to produce energy in the form of ATP, with only a small proportion of pyruvate instead converted to lactate, catalysed by lactate dehydrogenase (LDH), and exported from the cell. However, in malignant cells the majority of pyruvate is converted to lactate, even in the presence of abundant oxygen[44–46]. The ratio of glucose consumption:lactic acid production shown in Fig. 6 is close to 1:2, indicating these cells are converting the majority, if not all, of the glucose into lactate, consistent with the aerobic glycolysis frequently described as characteristic for HCC and across cancer types [1,44]. Similar results have been described in MCF-7 cells using microfluidic NMR, where more than twice the number of glucose molecules consumed were converted to lactic acid, suggesting stores of glucose within the cell from earlier culture were also converted [11]. The flux of lactate has also been shown to strongly correlate with tumour proliferation *in vivo*, even before a volumetric change of tumour size can be detected, suggesting this readout could be used as an early biomarker of disease progression [47].

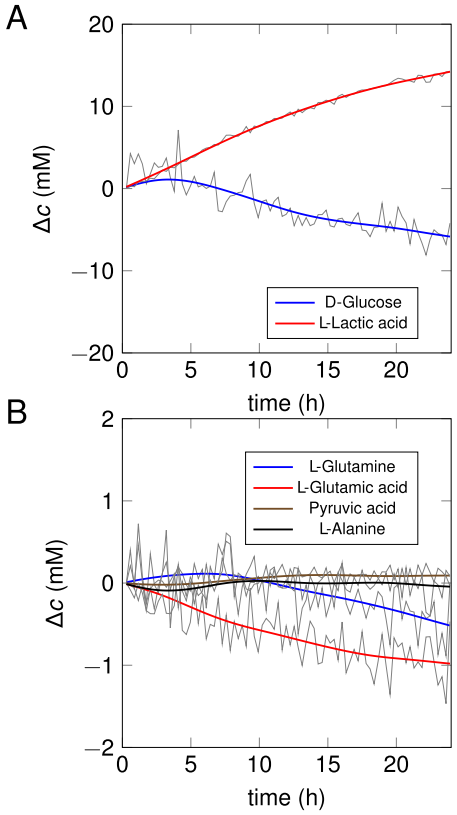

Fig. 6. Concentration changes as a function of time in a microfluidic culture of PLC cells. The narrow gray lines indicate concentrations determined directly from the sequence of acquired NMR spectra; the strong solid lines are the filtered data after Tikhonov regularisation. A: D-Glucose and L-Lactic acid; B: Other metabolites.

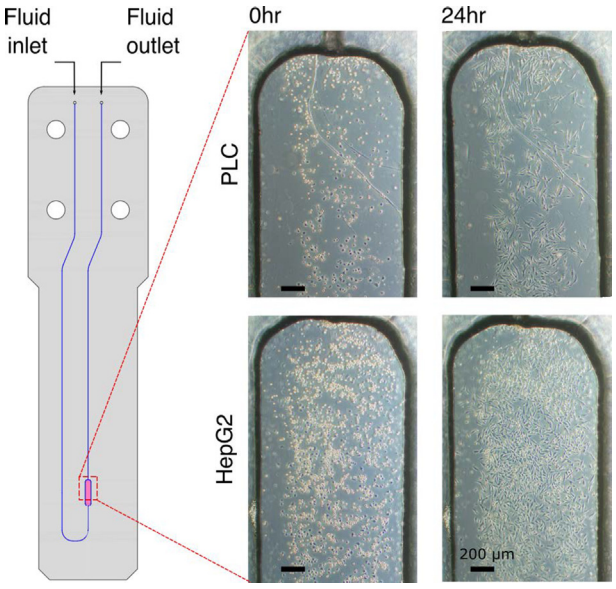

Fig. 5. Microscope images of the sample chamber for cell counts of PLC and HepG2 at 0hr and 24hr.

Glutamine and glutamic acid concentration are shown to decrease, likely due to a combination of glutamine degradation and uptake by the cells. Pyruvic acid is an intracellular intermediate molecule and therefore the lack of change observed is to be expected in this primarily extracellular measurement. Alanine showed a small decrease in extracellular concentration at the beginning of the experiment before it plateaued, possibly due to a low concentration of alanine in the media. Consumption of alanine, along with other amino acids, is necessary for biosynthesis of proteins in these rapidly growing cells. Alanine can be produced in cells via transamination of pyruvate by alanine aminotransferase (ALT). However, as previously explained, the majority of pyruvate in HCC/malignant cells is converted to lactate which reduces availability for alanine production. Dou et al. showed that the ratio of alanine to lactate production is reduced in highly proliferating HCC. This may mean that HCC cells are more dependent on extracellular alanine [47].

In principle, it is possible to obtain the metabolic conversion rate per cell from the measured data. However, this is complicated somewhat by the proliferation of the cells. We have addressed this by recording cell numbers from images of the sample chamber taken at 0hrs and 24hrs (Fig. 5), summarised in Table 1 to allow for estimation of cell proliferation and per cell calculations. Growth

Table 1
Cell numbers at 0 h and 24 h for each replicate experiment, used to determine metabolic rate per cell.

Sample	Type	0 h	24 h
1	PLC	1045	1027
2	PLC	499	537
3	PLC	639	785
4	HepG2	3255	2986

between these time points was assumed to be exponential. In some cases with greater initial cell number there was a small loss of cells, most likely as a result of over-confluence and acidosis.

For each sample, we thus obtained a vector of interpolated cell numbers $\mathbf{n}$ at each time point

$$n_k = n_0 e^{-\alpha t_k}, \tag{1}$$

where α is the growth rate determined by cell counting, and t_k signifies the time of acquisition of the k-th spectrum. The cumulative change in concentration for each metabolite $\delta_m(t)$ is related to the cell number and the (instantaneous) metabolic rate $p_m(t)$ per cell as:

$$\delta_m(t) = \int_0^t n(t) \cdot p_m(t) \mathrm{d}\tau. \tag{2}$$

In the present context, it makes sense to discretize this relationship on the time points of the individual NMR spectra, t_k. We thus obtain a matrix $\mathbf{B}$, each column of which contains the concentration changes of a particular metabolite over the duration of the experiment. The metabolic rates per cell can be arranged in the same way in a matrix $\mathbf{P}$. We then have

$$\mathbf{B} = \mathbf{N}\mathbf{P}, \tag{3}$$

where $\mathbf{N}$ is an upper triangular matrix that contains the interpolated cell numbers $n_k = n(t_k)$ as follows:

$$\mathbf{N} = \Delta t \begin{pmatrix} n_1 & 0 & 0 & \dots \\ n_1 & n_2 & 0 & \dots \\ n_1 & n_2 & n_3 & \dots \\ \vdots & \vdots & \vdots & \ddots \end{pmatrix}. \tag{4}$$

Formally, the metabolic rates $\mathbf{P}$ can be obtained by inversion of the linear relationship (3). However, due to the experimental noise contained in the concentration changes $\mathbf{B}$, this is numerically unstable. We therefore resort to Tikhonov regularisation, and obtain the metabolic rates as follows:

$$\mathbf{P} = \left(\mathbf{N}^T\mathbf{N} + \xi^2\mathbf{D}^T\mathbf{D}\right)^{-1}\mathbf{N}^T\mathbf{B}, \tag{5}$$

where ξ is the smoothing time window, and $\mathbf{D}$ is the discrete time derivative matrix

$$\mathbf{D} = \frac{1}{\Delta t}\begin{pmatrix} -1 & 1 & 0 & 0 & \dots \\ 0 & -1 & 1 & 0 & \dots \\ 0 & 0 & -1 & 1 & \dots \\ \vdots & \vdots & \vdots & \vdots & \ddots \end{pmatrix}. \tag{6}$$

The parameter ξ is chosen to produce a fit to the metabolic concentration changes (Fig. 6) that accurately tracks the data, but avoids following random fluctuations. A value of $\xi = 2000\,\mathrm{h}^2$ was found to be optimal. This leads to the metabolic rates shown for the PLC cells in Fig. 7. Metabolic rates of three PLC samples were determined and the mean and standard deviation reported, represented by solid lines and shaded error bands respectively. These results indicate an induction period for glucose uptake and a steadily increasing consumption rate from 0-8 h. This was not reflected in the lactic acid production. However, both glucose and lactic acid show a marked reduction in consumption/production rate in the latter two thirds of the experiment, likely due to the induction of acidosis and competition for limited remaining nutrients. This self inhibiting system is reflected in the reported amino acids L-Alanine and L-Glutamic acid, as they each slow in metabolic rate.

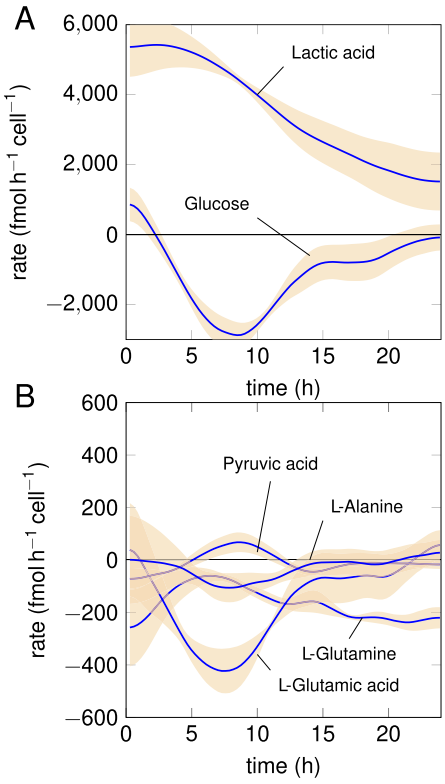

Fig. 7. Metabolic rates obtained from the concentration changes and the cell counts of PLC culture. Solid lines:mean, orange band: standard deviation.

5. Conclusions

We have demonstrated a novel system for *in operando* culture and metabolic analysis of live cells. We have shown that cancer cell lines can be grown on this microfluidic platform for 24 h and, with appropriate degassing, mM concentrations can be quantified from μL volumes. The continuous culture enabled by this system provides time-resolved data, enabling metabolic rates per hour to be readily observed from as few as 500 cells.

Data availability

Data will be made available on request.

Declaration of Competing Interest

The authors declare that they have no known competing financial interests or personal relationships that could have appeared to influence the work reported in this paper.

Acknowledgements

This work has been supported by the 'HUNTER' accelerator award from CRUK and the Institute for Life Sciences as part of the University of Southampton. This project has also received funding from EPSRC Grant No. EP/W020343/1.

References

[1] O. Warburg, On the origin of cancer cells, Science 123 (3191) (1956) 309–314, publisher: American Association for the Advancement of Science. https://doi.org/10.1126/science.123.3191.309. https://www.science.org/doi/10.1126/science.123.3191.309.

[2] U.E. Martinez-Outschoorn, M. Peiris-Pagés, R.G. Pestell, F. Sotgia, M.P. Lisanti, Cancer metabolism: a therapeutic perspective, Nature Revi. Clin. Oncol. 14 (1) (2017) 11–31, number: 1 Publisher: Nature Publishing Group. https://doi.org/10.1038/nrclinonc.2016.60. https://www.nature.com/articles/nrclinonc.2016.60.

[3] Y. Zhao, E.B. Butler, M. Tan, Targeting cellular metabolism to improve cancer therapeutics, Cell Death Disease 4 (3) (2013) e532–e532, number: 3 Publisher: Nature Publishing Group. https://doi.org/10.1038/cddis.2013.60. https://www.nature.com/articles/cddis201360.

[4] W. Bogner, R. Otazo, A. Henning, Accelerated MR spectroscopic imaging—a review of current and emerging techniques, NMR Biomed. 34 (5) (2021) e4314, _eprint: https://onlinelibrary.wiley.com/doi/pdf/10.1002/nbm.4314. https://doi.org/10.1002/nbm.4314. https://onlinelibrary.wiley.com/doi/abs/10.1002/nbm.4314.

[5] J. Wang, J. Weygand, K.-P. Hwang, A.S.R. Mohamed, Y. Ding, C.D. Fuller, S.Y. Lai, S.J. Frank, J. Zhou, Magnetic resonance imaging of glucose uptake and metabolism in patients with head and neck cancer, Sci. Rep. 6 (1) (2016) 30618, number: 1 Publisher: Nature Publishing Group. https://doi.org/10.1038/srep30618. https://www.nature.com/articles/srep30618.

[6] G. Hangel, C. Cadrien, P. Lazen, J. Furtner, A. Lipka, E. Hecková, L. Hingerl, S. Motyka, S. Gruber, B. Strasser, B. Kiesel, M. Mischkulnig, M. Preusser, T. Roetzer, A. Wöhrer, G. Widhalm, K. Rössler, S. Trattnig, W. Bogner, High-resolution metabolic imaging of high-grade gliomas using 7t-CRT-FID-MRSI, NeuroImage: Clinical 28 (2020) 102433, https://doi.org/10.1016/j.nicl.2020.102433, URL https://www.sciencedirect.com/science/article/pii/S2213158220302709.

[7] Z. Serber, A.T. Keatinge-Clay, R. Ledwidge, A.E. Kelly, S.M. Miller, V. Dötsch, High-Resolution Macromolecular NMR Spectroscopy Inside Living Cells, J. Am. Chem. Soc. 123 (10) 2446–2447. https://doi.org/10.1021/ja0057528. https://pubs.acs.org/doi/10.1021/ja0057528.

[8] G. Siegal, P. Selenko, Cells, drugs and NMR, J. Magn. Reson. 306 (2019) 202–212, https://doi.org/10.1016/j.jmr.2019.07.018, URL https://www.sciencedirect.com/science/article/pii/S1090780719301442.

[9] D. Lane, Y. Liaghati Mobarhan, R. Soong, P. Ning, W. Bermel, M. Tabatabaei Anaraki, B. Wu, H. Heumann, M. Gundy, H. Boenisch, T.-Y. Jeong, V. Kovacevic, M.J. Simpson, A.J. Simpson, Understanding the Fate of Environmental Chemicals Inside Living Organisms: NMR-Based 13C Isotopic Suppression Selects Only the Molecule of Interest within 13C-Enriched Organisms, Anal. Chem. 91 (23) (2019) 15000–15008, publisher: American Chemical Society. https://doi.org/10.1021/acs.analchem.9b03596.

[10] D. Lane, W. Bermel, P. Ning, T.-Y. Jeong, R. Martin, R. Soong, B. Wu, M. Tabatabaei-Anaraki, H. Heumann, M. Gundy, H. Boenisch, A. Adamo, G. Arhonditsis, A.J. Simpson, Targeting the Lowest Concentration of a Toxin That Induces a Detectable Metabolic Response in Living Organisms, Time-Resolved In Vivo 2D NMR during a Concentration Ramp, Analytical Chemistry, 92, American Chemical Society, 2020, pp. 9856–9865, https://doi.org/10.1021/acs.analchem.0c01370.

[11] B. Patra, M. Sharma, W. Hale, M. Utz, Time-resolved non-invasive metabolomic monitoring of a single cancer spheroid by microfluidic NMR, Sci. Rep. 11 (2021) 53, https://doi.org/10.1038/s41598-020-79693-1, URL https://www.ncbi.nlm.nih.gov/pmc/articles/PMC7794408/.

[12] L. Breindel, C. DeMott, D.S. Burz, A. Shekhtman, Real-time in-cell nuclear magnetic resonance: Ribosome-targeted antibiotics modulate quinary protein interactions, Biochemistry 57 (5) (2018) 540–546, publisher: American Chemical Society. https://doi.org/10.1021/acs.biochem.7b00938.

[13] M.T. Santini, G. Rainaldi, R. Romano, A. Ferrante, S. Clemente, A. Motta, P.L. Indovina, FEBS Lett. 557 (1–3) (2004) 148–154, https://doi.org/10.1016/S0014-5793(03)01466-2, URL https://febs.onlinelibrary.wiley.com/doi/abs/10.1016/S0014-5793%2803%2901466-2.

[14] U. Pilatus, E. Aboagye, D. Artemov, N. Mori, E. Ackerstaff, Z.M. Bhujwalla, Real-time measurements of cellular oxygen consumption, pH, and energy metabolism using nuclear magnetic resonance spectroscopy, Magnetic Reson. Med. 45 (5) (2001) 749–755, _eprint: https://onlinelibrary.wiley.com/doi/pdf/10.1002/mrm.1102. https://doi.org/10.1002/mrm.1102. https://onlinelibrary.wiley.com/doi/abs/10.1002/mrm.1102.

[15] A. Manz, G. Simone, J.S. O'Connor, P. Neuzil, Microfluidics and Lab-on-a-Chip, Royal Society of Chemistry, 2020.

[16] N. Azizipour, R. Avazpour, D.H. Rosenzweig, M. Sawan, A. Ajji, Evolution of biochip technology: A review from lab-on-a-chip to organ-on-a-chip, Micromachines 11 (6) (2020) 599, number: 6 Publisher: Multidisciplinary Digital Publishing Institute. https://doi.org/10.3390/mi11060599. https://www.mdpi.com/2072-666X/11/6/599.

[17] S.E. Park, A. Georgescu, D. Huh, Organoids-on-a-chip, Science 364 (6444) (2019) 960–965, https://doi.org/10.1126/science.aaw7894.

[18] C.M. Leung, P. de Haan, K. Ronaldson-Bouchard, G.-A. Kim, J. Ko, H.S. Rho, Z. Chen, P. Habibovic, N.L. Jeon, S. Takayama, M.L. Shuler, G. Vunjak-Novakovic, O. Frey, E. Verpoorte, Y.-C. Toh, A guide to the organ-on-a-chip, Nature Rev. Methods Primers 2 (1) (2022) 1–29, https://doi.org/10.1038/s43586-022-00118-6.

[19] Z. Sun, Q. Ji, A.R. Evans, M.J. Lewis, J. Mo, P. Hu, High-throughput LC-MS quantitation of cell culture metabolites, Biologicals 61 (2019) 44–51, https://doi.org/10.1016/j.biologicals.2019.07.003, URL https://www.sciencedirect.com/science/article/pii/S1045105619300788.

[20] J.K. Caines, D.A. Barnes, M.D. Berry, The use of seahorse XF assays to interrogate real-time energy metabolism in cancer cell lines, in: S.L. Christian (Ed.), Cancer Cell Biology: Methods and Protocols, Methods in Molecular Biology, Springer, US, 2022, pp. 225–234, https://doi.org/10.1007/978-1-0716-2376-3_17.

[21] T. TeSlaa, M.A. Teitell, Techniques to monitor glycolysis, Methods Enzymol. 542 (2014) 91–114, https://doi.org/10.1016/B978-0-12-416618-9.00005-4, URL https://www.ncbi.nlm.nih.gov/pmc/articles/PMC4276425/.

[22] A. Steiner, S.A. Schmidt, C.S. Fellmann, J. Nowak, C.-L. Wu, A.S. Feldman, M. Beer, L.L. Cheng, Ex vivo high-resolution magic angle spinning (HRMAS) 1h NMR spectroscopy for early prostate cancer detection, Cancers 14 (9) (2022) 2162, number: 9 Publisher: Multidisciplinary Digital Publishing Institute. https://doi.org/10.3390/cancers14092162. https://www.mdpi.com/2072-6694/14/9/2162.

[23] A. Skorupa, M. Ponski, M. Ciszek, B. Cichon, M. Klimek, A. Witek, S. Pakulo, L. Boguszewicz, M. Sokól, Grading of endometrial cancer using 1h HR-MAS NMR-based metabolomics, Sci. Reports 11 (1) (2021) 18160, number: 1 Publisher: Nature Publishing Group. https://doi.org/10.1038/s41598-021-97505-y. https://www.nature.com/articles/s41598-021-97505-y.

[24] J. Bart, J.W.G. Janssen, P.J.M. van Bentum, A.P.M. Kentgens, J.G.E. Gardeniers, Optimization of stripline-based microfluidic chips for high-resolution NMR, J. Magn. Reson. 201 (2) (2009) 175–185, https://doi.org/10.1016/j.jmr.2009.09.007, URL http://www.sciencedirect.com/science/article/pii/S1090780709002638.

[25] M. Sharma, M. Utz, Modular transmission line probes for microfluidic nuclear magnetic resonance spectroscopy and imaging, J. Magn. Reson. 303 (2019) 75–81, https://doi.org/10.1016/j.jmr.2019.04.007, URL http://www.sciencedirect.com/science/article/pii/S1090780719300655.

[26] N. Spengler, J. Höfflin, A. Moazenzadeh, D. Mager, N. MacKinnon, V. Badilita, U. Wallrabe, J.G. Korvink, Heteronuclear Micro-Helmholtz Coil Facilitates Mm-Range Spatial and Sub-Hz Spectral Resolution NMR of nL-Volume Samples on Customisable Microfluidic Chips, Plos One 11 (1) (2016) e0146384, https://doi.org/10.1371/journal.pone.0146384, URL https://plos.org/10.1371/journal.pone.0146384.

[27] V. Badilita, R.C. Meier, N. Spengler, U. Wallrabe, M. Utz, J.G. Korvink, Microscale nuclear magnetic resonance: A tool for soft matter research, Soft Matter 8 (41) (2012) 10583–10597, https://doi.org/10.1039/c2sm26065d, URL http://xlink.rsc.org/?DOI=c2sm26065d.

[28] A. Kalfe, A. Telfah, J. Lambert, R. Hergenröder, Looking into living cell systems: planar waveguide microfluidic NMR detector for in vitro metabolomics of tumor spheroids, Anal. Chem. 87 (14) (2015) 7402–7410, https://doi.org/10.1021/acs.analchem.5b01603, URL http://pubs.acs.org/doi/abs/10.1021/acs.analchem.5b01603.

[29] B. Patra, M. Sharma, W. Hale, M. Utz, Time-resolved non-invasive metabolomic monitoring of a single cancer spheroid by microfluidic NMR, Sci. Rep. 11 (1) (2021) 53, https://doi.org/10.1038/s41598-020-79693-1, URL https://www.nature.com/articles/s41598-020-79693-1.

[30] L. Zhuang, R.J. Fulton, P. Rettman, A.E. Sayan, J. Coad, A. Al-Shamkhani, S.I. Khakoo, Activity of IL-12/15/18 primed natural killer cells against hepatocellular carcinoma, Hep. Intl. 13 (1) (2019) 75–83, https://doi.org/10.1007/s12072-018-9909-3.

[31] Liver cancer statistics, library Catalog: www.cancerresearchuk.org. https://www.cancerresearchuk.org/health-professional/cancer-statistics/statistics-by-cancer-type/liver-cancer.

[32] E. Breous, R. Thimme, Potential of immunotherapy for hepatocellular carcinoma, J. Hepatol. 54 (4) (2011) 830–834, publisher: Elsevier. https://doi.org/10.1016/j.jhep.2010.10.013. https://www.journal-of-hepatology.eu/article/S0168-8278(10)00966-9/abstract.

[33] S. Cassim, J. Pouyssegur, Tumor microenvironment: A metabolic player that shapes the immune response, Int. J. Mol. Sci. 21 (1) (2020) 157, number: 1 Publisher: Multidisciplinary Digital Publishing Institute. https://doi.org/10.3390/ijms21010157. https://www.mdpi.com/1422-0067/21/1/157.

[34] I. Terrén, A. Orrantia, J. Vitallé, O. Zenarruzabeitia, F. Borrego, NK cell metabolism and tumor microenvironment, Fron. Immunol. 10 (2019), URL https://www.frontiersin.org/articles/10.3389/fimmu.2019.02278.

[35] K. Renner, K. Singer, G.E. Koehl, E.K. Geissler, K. Peter, P.J. Siska, M. Kreutz, Metabolic hallmarks of tumor and immune cells in the tumor microenvironment, Front. Immunol. 8 (2017), URL https://www.frontiersin.org/article/10.3389/fimmu.2017.00248.

[36] M. Sharma, M. Utz, Modular transmission line probes for microfluidic nuclear magnetic resonance spectroscopy and imaging, J. Magn. Reson. 303 (2019) 75–81, https://doi.org/10.1016/j.jmr.2019.04.007, URL http://www.sciencedirect.com/science/article/pii/S1090780719300655.

[37] A. Yilmaz, M. Utz, Characterisation of oxygen permeation into a microfluidic device for cell culture by in situ NMR spectroscopy, Lab Chip 16 (11) (2016) 2079–2085, https://doi.org/10.1039/C6LC00396F, URL https://pubs.rsc.org/en/content/articlelanding/2016/lc/c6lc00396f.

[38] J.A. Aguilar, M. Nilsson, G. Bodenhausen, G.A. Morris, Spin echo NMR spectra without J modulation, Chem. Commun. 48 (6) (2011) 811–813, https://doi.org/10.1039/C1CC16699A, URL https://pubs.rsc.org/en/content/articlelanding/2012/cc/c1cc16699a.

[39] J. Bezanson, A. Edelman, S. Karpinski, V.B. Shah, Julia: A Fresh Approach to Numerical Computing, SIAM Rev. 59 (1) (2017) 65–98, https://doi.org/10.1137/141000671, URL https://epubs.siam.org/doi/abs/10.1137/141000671.
[40] G.R. Finch, Ph.D. thesis, University of Southampton (2017). [link]. http://eprints.soton.ac.uk/id/eprint/409692.
[41] S. Heeneman, N.E.P. Deutz, W.A. Buurman, The concentrations of glutamine and ammonia in commercially available cell culture media, J. Immunol. Methods 166 (1) (1993) 85–91, https://doi.org/10.1016/0022-1759(93)90331-Z, URL https://www.sciencedirect.com/science/article/pii/002217599390331Z.
[42] D.S. Wishart, Y.D. Feunang, A. Marcu, A.C. Guo, K. Liang, R. Vázquez-Fresno, T. Sajed, D. Johnson, C. Li, N. Karu, Z. Sayeeda, E. Lo, N. Assempour, M. Berjanskii, S. Singhal, D. Arndt, Y. Liang, H. Badran, J. Grant, A. Serra-Cayuela, Y. Liu, R. Mandal, V. Neveu, A. Pon, C. Knox, M. Wilson, C. Manach, A. Scalbert, HMDB 4.0: The human metabolome database for 2018, Nucleic Acids Res 46 (D1) (2018) D608–D617, https://doi.org/10.1093/nar/gkx1089, URL https://academic.oup.com/nar/article/46/D1/D608/4616873.
[43] D.G. Tenen, L. Chai, J.L. Tan, Metabolic alterations and vulnerabilities in hepatocellular carcinoma, Gastroenterol. Report 9 (1) (2021) 1–13, https://doi.org/10.1093/gastro/goaa066.
[44] E.M. Palsson-McDermott, L.A.J. O'Neill, The warburg effect then and now: From cancer to inflammatory diseases, BioEssays 35 (11) (2013) 965–973, _eprint: https://onlinelibrary.wiley.com/doi/pdf/10.1002/bies.201300084. https://doi.org/10.1002/bies.201300084. https://onlinelibrary.wiley.com/doi/abs/10.1002/bies.201300084.
[45] H. Tian, X. Zhu, Y. Lv, Y. Jiao, G. Wang, Glucometabolic reprogramming in the hepatocellular carcinoma microenvironment: Cause and effect, Cancer Manage. Res. 12 5957–5974. https://doi.org/10.2147/CMAR.S258196. https://www.ncbi.nlm.nih.gov/pmc/articles/PMC7381782/.
[46] M. Mossenta, D. Busato, M. Dal Bo, G. Toffoli, Glucose metabolism and oxidative stress in hepatocellular carcinoma: Role and possible implications in novel therapeutic strategies, Cancers 12 (6) 1668, number: 6 Publisher: Multidisciplinary Digital Publishing Institute. https://doi.org/10.3390/cancers12061668. https://www.mdpi.com/2072-6694/12/6/1668.
[47] Q. Dou, A.K. Grant, C. Callahan, P. Coutinho de Souza, D. Mwin, A.L. Booth, I. Nasser, M. Moussa, M. Ahmed, L.L. Tsai, PFKFB3-mediated pro-glycolytic shift in hepatocellular carcinoma proliferation, Cell. Mol. Gastroenterol. Hepatol. 15 (1) (2022) 61–75, https://doi.org/10.1016/j.jcmgh.2022.09.009, URL https://www.ncbi.nlm.nih.gov/pmc/articles/PMC9672450/.